



1 The El Niño event of 2015-16: Climate anomalies and their impact on groundwater
2 resources in East and Southern Africa

3 Seshagiri Rao Kolusu¹, Mohammad Shamsudduha^{2,3}, Martin C Todd¹, Richard G Taylor³,
4 David Seddon³, Japhet J Kashaigili⁴, Girma Y Ebrahim⁵, Mark O Cuthbert^{3,6}, James P R
5 Sorensen⁷, Karen G Villholth⁵, Alan M MacDonald⁸, and Dave A MacLeod⁹

6
7 1. Department of Geography, University of Sussex, Brighton, BN1 9QS, UK
8 s.kolusu@sussex.ac.uk

9 2. Institute for Risk and Disaster Reduction, University College London, Gower Street,
10 London WC1E 6BT, UK

11 3. Department of Geography, University College London, Gower Street, London WC1E
12 6BT UK

13 4. Sokoine University of Agriculture, Morogoro, Tanzania

14 5. International Water Management Institute, Pretoria, South Africa

15 6. School of Earth and Ocean Sciences, Cardiff University, Main Building, Park Place,
16 Cardiff, CF10 3AT, UK

17 7. British Geological Survey, Maclean Building, Crowmarsh Gifford, Wallingford,
18 Oxfordshire OX10 8BB UK

19 8. British Geological Survey, The Lyell Centre, Research Avenue South, Edinburgh
20 EH14 4AP UK

21 9. Oxford University, Atmospheric, Oceanic and Planetary Physics, UK

22
23
24 **Keywords**

25
26 El Nino; ENSO; Climate; groundwater; Africa; sustainability; recharge; climate impacts; water
27 management; GRACE

28



29 Abstract

30

31 The impact of climate variability on groundwater storage has received limited attention despite
32 widespread dependence on groundwater as a resource for drinking water, agriculture and
33 industry. Here, we assess the climate anomalies that occurred over Southern Africa (SA) and
34 East Africa, south of the equator (EASE), during the major El Niño event of 2015-16, and their
35 associated impacts on groundwater storage, across scales, through analysis of in situ
36 groundwater piezometry and GRACE satellite data. At the continental scale, the El Niño of
37 2015-16 was associated with a pronounced dipole of opposing rainfall anomalies over EASE
38 and Southern Africa, north/south of $\sim 12^{\circ}\text{S}$, a characteristic pattern of ENSO. Over Southern
39 Africa the most intense drought event in the historical record occurred, based on an analysis of
40 the cross-scale areal intensity of surface water balance anomalies (as represented by the
41 Standardised Precipitation-Evapotranspiration Index, SPEI), with an estimated return period of
42 at least 200 years and a best estimate of 260 years. Climate risks are changing and we estimate
43 that anthropogenic warming only (ignoring changes to other climate variables e.g.
44 precipitation) has approximately doubled the risk of such an extreme SPEI drought event.
45 These surface water balance deficits suppressed groundwater recharge, leading to a substantial
46 groundwater storage decline indicated by both GRACE satellite and piezometric data in the
47 Limpopo basin. Conversely, over EASE during the 2015-16 El Niño event, anomalously wet
48 conditions were observed with an estimated return period of ~ 10 years, likely moderated by
49 the absence of a strongly positive Indian Ocean Zonal Mode phase. The strong but not extreme
50 rainy season increased groundwater storage as shown by satellite GRACE data and rising
51 groundwater levels observed at a site in central Tanzania. We note substantial uncertainties in
52 separating groundwater from total water storage in GRACE data and show that consistency
53 between GRACE and piezometric estimates of groundwater storage is apparent when spatial
54 averaging scales are comparable. These results have implications for sustainable and climate-
55 resilient groundwater resource management, including the potential for adaptive strategies,
56 such as managed aquifer recharge during episodic recharge events.



57 1. Introduction

58

59 The El Niño-Southern Oscillation (ENSO) phenomenon is the dominant single driver of
60 climate variability and large-scale extremes across the tropics including most of Africa. Few
61 studies have investigated the hydrological impacts of ENSO events on groundwater despite its
62 vital role in sustaining ecosystem function as well as agricultural and domestic water supplies.
63 Here, we quantify climate anomalies and groundwater resources over Eastern Africa, South of
64 the Equator (EASE) and Southern Africa (SA), during the recent major El Niño event of 2015-
65 16, which in the Pacific sector was one of the biggest on record. El Niño is typically associated
66 with wet and dry anomalies over EASE and SA, respectively (Ropelowski and Halpert, 1987),
67 but with considerable diversity in this response among El Niño events (Supplementary
68 Information S1). Much of SA experienced extreme drought in 2015-16 with severe impacts on
69 local food security, livelihoods and key sectors of the economy (SADC 2016a; 2016b; Archer
70 *et al.*, 2017; Siderius *et al.*, 2018; Supplementary Information S1).

71

72 Groundwater is the dominant source of safe water for rural populations and many expanding
73 cities in EASE and SA (MacDonald *et al.*, 2012); in drylands, groundwater is often the only
74 perennial source of water. Although relatively under-developed to date, groundwater resources
75 are being developed rapidly in Africa (Taylor *et al.*, 2009; Calow *et al.*, 2010; Villholth *et al.*,
76 2013) and feature prominently in national development plans, especially to satisfy the need for
77 increased access to safe water and agricultural intensification under rapidly growing
78 populations and economic development. Groundwater is especially important in Africa where
79 surface runoff efficiency is lower than elsewhere (McMahon, 1987) and drinking of untreated
80 surface water is associated with poor health (Hunter *et al.*, 2010). The long-term viability of
81 groundwater withdrawals and the livelihoods and ecosystems that groundwater sustains depend
82 on recharge.

83

84 Unlike surface water, research evaluating associations between groundwater storage and
85 ENSO, or indeed other modes of climate variability is rather limited (e.g. Holman *et al.*, 2011,
86 Kuss and Gurdak, 2014), despite evidence that climate variability and extreme rainfall
87 preferentially drive or restrict groundwater recharge. Several studies have shown recharge to
88 be episodic in semi-arid regions of Africa (Meyer *et al.*, 2005, van Wyk *et al.*, 2011, Taylor *et*



89 *al.*, 2013, Cuthbert *et al.*, 2017) and elsewhere (Jasechko and Taylor, 2015, Cuthbert *et al.*,
90 2016), highlighting the need to understand patterns and drivers of climate variability both
91 temporarily and spatially, that influence recharge. Bonsor *et al.* (2018) analysed recent (2002-
92 2016) trends in, and seasonality of groundwater storage within 12 African sedimentary basins
93 implied from GRACE satellite data. Here, we employ evidence from both in situ observations
94 (piezometry) and GRACE satellite data to examine the effect of large-scale interannual climate
95 anomalies on groundwater across spatial scales for locations and domains that represent the
96 rainfall anomaly gradient over EASA and SA associated with characteristic El Niño response,
97 exemplified by the event of 2015-16. Beyond a few site-specific studies, the impacts of larger-
98 scale climate extremes on groundwater remain substantially unresolved. This hinders our
99 ability to determine acceptable levels of groundwater abstraction and depletion. This study
100 aims to quantify and understand the responses, during the 2015-16 El Niño of (i) the
101 surface/terrestrial water balance and (ii) groundwater storage over EASE and SA from regional
102 to local scales. Further, it seeks to place the 2015-16 El Niño event statistically in the historical
103 context.

104

105 **2. Data and methods**

106

107 2.1. Climate data and analysis

108

109 We analyse data over the broad region of Africa South of the Equator and over an extended
110 austral summer wet season of October-April, which encompasses the full wet season over SA
111 (excluding the Cape region) and those parts of EASA (south of ~5°S), which experience a
112 similarly annual unimodal rainfall regime (Dunning *et al.*, 2016), and will accommodate the
113 response time of groundwater systems to climate. This region also experiences a coherent
114 ENSO signal (Section 3.1). We use the Standardized Precipitation Evapotranspiration Index
115 (SPEI) (Vicente-Serrano *et al.*, 2010), which is a simple representation of surface water balance
116 anomalies, derived over this 7-month season (SPEI-7), described in Supplementary
117 Information S2. Note that some findings will be sensitive to the choice of drought index.

118

119 We assess the extent and intensity of SPEI-7 anomalies across two large sub-domains across
120 EASE (4-12°S, 30-40°E) and SA (10-35°S, 10-40°E). These domains are specified to (i)



encompass the anomalous wet and dry dipole conditions, respectively, typically experienced during El Niño events (figure S1(b)) and specifically in 2015-16 (figure 1(a)). (ii) Ensure common unimodal annual rainfall with Austral summer wet season (with the exception of the extreme southwest SA). For each domain, the areal extent and intensity of SPEI-7 was determined separately using Intensity-Areal-extent Frequency (IAF) curves of Mishra and Cherkauer (2010). IAF curves express the relationship between the intensity and areal extent of SPEI, allowing comparison between years, irrespective of the precise spatial location of dry/wet conditions within the domain. We estimate the return periods (Supplementary Information S3) of SPEI-7 IAFs observed during the 2015-16 and other El Niño event(s).

2.2 Groundwater storage estimates from GRACE satellite data

Regional-scale changes in groundwater storage (GWS) (2002-16) are estimated (Supplementary Information S4) from GRACE satellite measurements of total terrestrial water storage (TWS) anomalies, by subtracting changes in the other terrestrial stores, which, in our tropical region, comprise soil moisture (SMS) and surface water (SWS) stores (eq.1), themselves estimated from Land-Surface Model (LSM) simulations.

$$\Delta GWS = \Delta TWS - (\Delta SMS + \Delta SWS) \quad (\text{eq. 1})$$

Where Δ refers to the anomaly with respect to the long-term data series. To address uncertainty associated with different GRACE processing strategies and with derivation of ΔGWS , we apply an ensemble mean of three GRACE TWS estimates and four LSM product estimates of SMS and SWS, and we provide the associated uncertainty ranges for each term.

2.3 Groundwater storage estimates from piezometric observations

Groundwater level records were compiled in two sites situated at the heart of the two EASE/SA ENSO rainfall dipole centres of action (figure 1(a)) over the period of August 2002 to July 2016 (Supplementary Information S5): (i) The Makutapora wellfield (35.75°E, 5.90°S) in central Tanzania (EASE) where data from three stations were averaged, representing an area of ~60 km² (Taylor *et al.*, 2013); and (ii) the Limpopo Basin in SA (~28-32°E, 22.5-25°S), where data from 40 stations representing ~47,000 km² were averaged.



153 **3. Results and discussion**

154

155 3.1 Climate anomalies over EASE and SA during the 2015-16 El Niño event

156

157 *3.1.1 EASE/SA climate anomalies*

158

159 The 2015-16 El Niño was the second strongest event within the available ~165-year Pacific
 160 Ocean Sea Surface Temperature (SST) record, with SST anomalies exceeding 2°C for 6 months
 161 from October 2015 (figure S1(b)). By some measures 2015-16 was the strongest El Niño since
 162 1950 (Supplementary Information S1). Many of the observed climate anomalies around the
 163 world were typical of El Niño years (Blunden and Arndt 2016). Over our study region, a
 164 pronounced north-south dipole in SPEI-7 anomalies was observed (figure 1(a)), indicating
 165 intense and extensive drought over SA (negative SPEI-7) and the wetter than normal conditions
 166 over EASE (positive SPEI-7). In detail, most of SA south of 10°S experienced a substantial
 167 water balance deficit: exceptional drought (SPEI <-2) conditions were experienced over
 168 extensive parts of northern South Africa and northern Namibia, southern Botswana and
 169 Zambia, as well as most of Zimbabwe and southern Mozambique and Malawi (figure 1(a)).
 170 Most of EASE experienced above average rainfall during this period, with SPEI values >1
 171 across most of Tanzania, and a localised exceptionally wet region over the northernmost part
 172 of Mozambique. The Makutapora and Limpopo sites (figure 1(a)) are located in areas
 173 representative of the large-scale north/south rainfall dipole.

174

175 This spatial dipole pattern is very similar to the characteristic pattern of anomalies during El
 176 Niño across the region, as represented by the leading Empirical Orthogonal Function (EOF) of
 177 interannual variability (figure S1(b), Section S1) which correlates strongly with ENSO and
 178 Indian Ocean SSTs figure S1(c). Indeed, the EOF coefficient value for 2015-16 is the second
 179 highest within the entire 1901-2016 period. As such, across our study region 2015-16
 180 represents an extreme exemplar of the characteristic El Niño climate response. Of course, a
 181 complex set of planetary, regional and local scale processes related to, and independent of, El
 182 Niño are fully responsible for the observed anomalies (e.g. Blamey et al., 2018). The structure
 183 of the atmospheric anomalies, specifically the mean meridional overturning circulation
 184 associated with the large-scale SPEI-7 anomalies (figure 2(a)) shows large-scale anomalous



185 ascent over EASE between $\sim 0^\circ$ and 10°S indicative of enhanced deep convection, with
186 compensating descent over SA throughout the depth of the troposphere, which acts to suppress
187 convection. The low-level horizontal circulation (figure 2(b)) indicates key features associated
188 with the SPEI-7 dipole, notably: (i) An anomalous southerly flow from the southern Indian
189 Ocean into continental SA (Feature A in figure 2(b)), which weakens the transport of water
190 vapour from the humid tropical Indian Ocean leading to a decrease in moisture flux
191 convergence over SA. This is associated with a weakening of the mean ‘Mascarene’ subtropical
192 high over the Southern Indian Ocean (Feature B in figure 2(b)). (ii) Over EASE there are
193 anomalous low-level westerlies over Tanzania (Feature C in figure 2(b)), which weaken the
194 mean easterlies and enhance convergence over Tanzania, a structure characteristic of wet spells
195 (Berhane and Zaitchik, 2014; Nicholson 2017).

196
197 Groundwater recharge in the semi-arid tropics is favoured by high intensity rainfall events
198 (Owor, 2009; Jasechko and Taylor, 2015) within wet seasons, which may be modulated by
199 climate anomalies during El Niño conditions. During 2015-16, the intensities of the 80th
200 percentile of daily rainfall, a simple proxy of potential groundwater recharge-relevant rainfall,
201 increased by $\sim 1\text{--}5\text{ mm day}^{-1}$ across much of EASE (figure 1(b)), representing a 100-150%
202 increase in many places. Whilst the association of rainfall intensity and enhanced recharge
203 across large and heterogeneous regions remains to be resolved, this intensification of rainfall
204 is consistent with greater groundwater recharge. Across SA the magnitude of the 80th
205 percentile reduced by $\sim 1\text{--}2\text{ mm day}^{-1}$, potentially reducing groundwater recharge.

207 3.1.2. The 2015-16 event in the historical context

208
209 SPEI-7 IAF curves represent water balance anomalies across all spatial scales. For the SA
210 region, 2015/16 experienced the most extreme SPEI-7 drought within the historical period,
211 with an estimated IAF curve return period of ~ 260 years (range 190-290 years) (figure 3(a)).
212 The 2015-16 drought was of greater intensity than those during previous El Niño events of
213 comparable magnitude, 1997-98 and 1982-83, whose SPEI-7 IAF curve return periods are
214 estimated to be only ~ 6 years (range 4-9 years) and ~ 43 years (range 35-47 years),
215 respectively). The contrasting intensity of SA drought between these events highlights the
216 diversity in responses over EASE/SA to El Niño, related to both the different character of the



217 events in the Pacific sector (2015-16 was strongest in the central rather an East Pacific as in
218 1997-98, see Section S1), and the specific regional circulation features during these events
219 which modulate the diverse ENSO teleconnections to SA (Ratnam *et al.*, 2014; Blamey *et al.*,
220 2018). Moreover, the 2015-16 drought followed a moderate drought in 2014-15 (Blamey *et al.*,
221 2018), which had important implications for groundwater levels (Section 3.2.2), and
222 statistically this 2-year drought event remarkably unlikely. The extreme SPEI-7 anomalies over
223 SA in 2015-16 result from low rainfall and extremely high temperatures (Brundel and Arndt
224 2016, Russo *et al.*, 2016), potentially related to land-atmosphere feedback processes (e.g.
225 Seneviratne *et al.*, 2010), through reduced vegetation and soil moisture, perhaps persisting from
226 2014-15. Uncertainty in the strength of land-atmosphere coupling over SA remains high with
227 contradictory results from model analyses (e.g. Koster *et al.*, 2008) and combined observation-
228 model analysis (Ferguson *et al.*, 2012), suggesting weak and strong coupling, respectively.
229 Further, warming across SA in recent decades can be attributed substantially to anthropogenic
230 radiative forcing (Bindoff *et al.*, 2013). As such climate risks are changing. We estimate that
231 the risk of a 2015-16 magnitude SPEI-7 drought over SA to have increased by approximately
232 two times due to the effects purely of anthropogenic warming, ignoring changes to other
233 climate variables and variability (see Supplementary Information S3). Other drought indices
234 may have differing sensitivities to temperature.

235

236 Over the EASE domain as a whole, the 2015-16 event was wet but not extreme, with an SPEI-
237 7 IAF curve estimated return period (figure 3(b)) of only ~10 years (range 5-12 years). The
238 anomalies were far weaker than that during the 1997-98 El Niño (figure 3b). These differences
239 may be associated with the state of the Indian Ocean Zonal Model (IOZM), an east-west
240 structure of coupled ocean-atmosphere circulation, influencing convection and rainfall over
241 East Africa (Saji *et al.*, 1999, Supplementary Information S1). The 1997-98 El Niño coincided
242 with a very strong positive IOZM event, unlike that of 2015-16, in which the IOZM was weakly
243 positive. Indeed, the wettest EASE year on record, 1961-1962, experienced a very strongly
244 positive IOZM event but no El Niño event (Nicholson, 2015).

245

246 3.2 Impact of 2015-16 climate anomalies on groundwater storage

247

248 3.2.1 Large-scale estimates of ΔTWS , ΔSMS , ΔSWS and ΔGWS



249

250 Regionally, GRACE ensemble-mean Δ TWS anomalies (figure 4(a)), and estimated Δ GWS (eq.
251 1, figure 4(d)), for 2015-16 reflect the north-south dipole over EASE/SA associated with the
252 El Niño-related SPEI-7 climate anomalies (figure 1(a)). Positive Δ TWS and Δ GWS anomalies
253 exist north of $\sim 10^\circ\text{S}$ across EASE (including the Makutapora site), the central DRC and
254 northern Angola. Negative Δ TWS and Δ GWS anomalies occur over an extensive region of
255 eastern SA including the Limpopo site. However, despite broad-scale structural similarity,
256 there are some apparent inconsistencies between Δ TWS (and other components of the water
257 budget, including Δ GWS) and the SPEI-7 climate signal that we consider below.

258

259 Viewed more closely, the partitioning of large-scale Δ TWS anomalies between the modelled
260 Δ SMS, Δ SWs and residual Δ GWS is spatially complex. First, we note that Δ SWs (figure 4(c))
261 plays only a minor role across the domain. Further, the coherence of the spatial structure in
262 anomalies in Δ SMS (figure 4(b)) is much less clear than for Δ TWS, reflecting uncertainties in
263 soil moisture among individual LSMs, as highlighted by Scanlon *et al.* (2018). Then,
264 considering the drought region over SA, a number of features emerge. (i) The relative
265 magnitude of Δ TWS deficits over South Africa are less than those of the SPEI-7, compared to
266 the northern more humid parts of SA (compare figures 4(a) and 1(a)). This difference may be
267 expected since Δ TWS is an absolute measure of water volume whereas SPEI-7 is a standardised
268 anomaly relative to climate. Consequently, these measures may be expected to diverge across
269 mean rainfall gradients. Further, SPEI-7 reflects potential rather than actual evapotranspiration.
270 (ii) Over the northern sector of Zambia, Zimbabwe and Malawi the strongly negative Δ TWS
271 anomaly is almost equally shared between modelled reductions in Δ SMS and Δ GWS. (iii) To
272 the south over South Africa however, the (rather weaker) Δ TWS deficits are effectively
273 accounted for by Δ SMS anomalies such that Δ GWS anomalies are actually close to zero or
274 indeed slightly positive. The Limpopo study site lies at a transition zone between regions with
275 apparently strongly reduced Δ GWS to the northeast and close to zero or slightly positive
276 Δ GWS to the southwest. As geology is broadly continuous across the region, the transition is
277 largely related to uncertainty in the estimation of modelled Δ SMS.

278

279 Considering the anomalous wet region over EASE to the north of $\sim 10^\circ\text{S}$, Δ GWS broadly
280 mirrors the structure of Δ TWS, but the detailed picture is complex. Over most of Tanzania and



281 Angola positive Δ TWS anomalies are largely partitioned into the Δ GWS rather than Δ SMS,
282 whereas over southern DRC the reverse is the case. Moreover, there are interesting apparent
283 contradictions between the climate SPEI-7 and GRACE Δ TWS data. Over Namibia and
284 southern Angola, negative SPEI-7 (figure 1(a) and Δ SMS, figure 4(b)) coincides with positive
285 Δ TWS anomalies (figure 4(a)) leading to very strong positive Δ GWS anomalies (figure 4(d))
286 that are inconsistent with climate anomalies from SPEI-7. Conversely, and more locally, over
287 northern Mozambique, a positive Δ SMS anomaly, resulting from the driving rainfall data (see
288 the SPEI-7 wet anomaly, figure 1(a)) is not reflected in a strong Δ TWS signal, which leaves a
289 counterintuitive, negative residual response in Δ GWS. As such, GRACE Δ GWS exhibits
290 inconsistent responses to both apparent anomalous dry and wet conditions, likely to be a result
291 of limitations in observational precipitation data and LSMs.

292

293 3.2.2 *In situ and GRACE-derived estimates of Δ GWS at the Makutapora and Limpopo Basins*

294

295 Piezometry for the two observatory sites and changes in GWS estimated from GRACE and
296 LSMs are shown in figure 5. First, we note that uncertainty in the mean GRACE Δ GWS
297 estimate (blue shading around blue line in figures 5(a) and 5(b)), whilst often large, is generally
298 smaller than the signals of inter-annual variability which are the main focus of our analysis.
299 However, variability in mean GRACE Δ GWS within recharge seasons is small relative to
300 uncertainty, such that we cannot confidently draw inferences at these timescales.

301

302 Specifically, at the SA Limpopo site, observed piezometry (figure 5(a)) shows an annual cycle
303 in GWS in most years with a ‘saw tooth’ pattern representing steady recessions in GWS during
304 the dry season from May to October followed by rapid increases typically starting in December
305 in response to the onset of the wet season to peak post-wet season in April (lagging peak rainfall
306 by ~1-2 months). GWS in 2015-16 is well below average with a seasonal but subdued GWS
307 rise delayed (until March) due to the highly anomalous early wet season drought. The GWS
308 rise in March-April following rains in March is the second smallest on record; only 2002-3 has
309 lower seasonal increase in GWS. The 2015-16 drought is preceded by negligible recharge in
310 the dry year of 2014-15 (figure 5(a)), such that GWS as of mid-2016 was lowest in the 14-year
311 record. As such, the major drought of 2015-16 compounded weak recharge in the previous year



312 to leave GWS at historically low levels. This may have been compounded by increased
313 abstractions during these dry years.

314

315 Comparison of piezometry and GRACE derived GWS, suggests a broad correspondence at
316 least when annually or seasonally averaged, ($r = 0.62$, significant at the 0.01 probability level).
317 The prolonged decline over 2014-16 is observed in both GRACE and piezometry. When
318 averaged over all years, the mean annual cycle is similar in phase and magnitude (not shown).
319 As such, at least broad temporal averaging scales GRACE is corroborated by piezometry at the
320 Limpopo site, where the scales of spatial averaging are similar. However, within-seasons, the
321 uncertainty in GRACE Δ GWS leads to a much 'noisier' mean signal at Limpopo which cannot
322 resolve the annual 'saw-tooth' pattern (figure 5(b)): in GRACE Δ GWS individual years have
323 a rather variable annual cycle despite a clear cycle in rainfall. Notably, the apparent strong rise
324 in Δ GWS during early season 2015-16, not corroborated by piezometry or rainfall coincides
325 with the greatest uncertainty within the record.

326

327 At the EASE Makutapora site, observed piezometric-GWS (figure 5(b)) shows little inter-
328 annual variability, with long periods of GWS recessions e.g. 2002-6, 2012-16, interrupted by
329 irregular and infrequent GWS increases, in declining order of magnitude 2006-7, 2009-10 and
330 2015-16, all El Niño years. The wet conditions in 2015-16 produced a major recharge event
331 though observed piezometric responses are smaller than in 2006-7 and 2009-10, despite higher
332 rainfall (figure 5(b)). Under highly dynamic pumping regimes (figure 5(c)), GWS changes are
333 only a partial proxy for groundwater recharge; the sharp increase (~50%) in wellfield pumping
334 in May 2015 served to diminish the response in piezometric-GWS to the 2015-16 El Niño.
335 Overall, however, the findings are consistent with the analysis of Taylor *et al.* (2013) who note
336 highly episodic recharge at Makutapora over the period since the 1960s associated with years
337 of heavy rainfall. The 2015-16 El Niño event represents a major event driving GWS at the
338 Makutapora wellfield, despite moderate rainfall anomalies over EASE.

339

340 There is only a rather general association between GRACE and piezometric estimates of
341 groundwater storage variability at the Makutapora site. The magnitude of major GRACE
342 increases in Δ GWS in individual years matches fairly well with the episodic piezometry events
343 of 2006-7, 2009-10 and 2015-16, although the second largest GRACE Δ GWS increase occurs



344 in 2014-15 with no response apparent in piezometry. Overall, the correlation of GRACE
345 Δ GWS and piezometric GWS of 0.51 is only moderate (significant at the 0.05 probability level)
346 but clearly reflects the low frequency multi-annual trends (at least up to 2013) as well as
347 interannual variability.

348

349 However, stark differences between GRACE and piezometry are apparent. In contrast to
350 piezometry, GRACE (figure 5(b)) shows increases in Δ GWS in almost every year (with lag of
351 ~ 1 month after the rainfall annual peak), suggesting recharge occurs annually, in contrast to
352 the piezometry. Further, GRACE Δ GWS replicates the low frequency recessionary trend over
353 the period 2002-07 but not since 2012. Resolving these contradictions is problematic but two
354 likely explanations emerge (i) Incommensurate scales of observation from piezometry (area
355 $\sim 60 \text{ km}^2$) and GRACE ($\sim 200,000 \text{ km}^2$). More localised processes may dominate the piezometry
356 record, perhaps including recharge sensitivity to contributions from local river and wetland
357 flooding in addition to rainfall. Further, the effects of local pumping will strongly influence the
358 piezometric record. This could explain the low frequency trend discrepancy, in which the
359 former period 2002-07 reflects a widespread groundwater recession, following the
360 anomalously high recharge during the El Niño event of 1997-98 (Taylor *et al.*, 2013), whilst
361 the recent accelerated trend reflects the effects of the rapid increase in abstraction, which may
362 have a more localised effect apparent only in the piezometric observations. As such the
363 piezometric record shows only episodic recharge whilst the GRACE indicated annual and
364 episodic recharge processes. (ii) Errors in GRACE Δ GWS resulting from inaccurate accounting
365 of Δ SMS and Δ SWS, which leaves a residual artefact of an annual positive Δ GWS signal, see
366 Section 3.1, Shamsudduha *et al.* (2017) and Scanlon *et al.* (2018). Such errors may not be
367 adequately accounted for in the uncertainty estimates in GRACE Δ GWS given for example the
368 similarity in LSM design and driving data. Indeed, at both the Limpopo and Makutapora sites,
369 we note stronger correlations between seasonal local rainfall and piezometric GWS than with
370 GRACE Δ GWS (not shown).

371

372 4. Concluding Discussion

373

374 We quantify the climate anomalies and groundwater response during the major El Niño event
375 of 2015-16, over Southern and Eastern Africa, south of the equator, across a range of spatial



376 scales from regional to local. Our analysis confirms that the event was associated with a
377 pronounced north/south dipole pattern of positive/negative rainfall and water balance
378 anomalies over EASE/SA, typical of the ENSO teleconnection to the region. It was the second
379 largest such dipole event on record since 1900. We must not overlook, however, the
380 considerable diversity in climate anomalies over Africa between El Niño events.

381

382 The response of the water balance including GWS to these climate anomalies is marked. Over
383 EASE, total rainfall and daily intensities were higher than normal and we estimate the return
384 period for the SPEI-7 water balance metric, over the domain as a whole, to be ~10 years. Wet
385 anomalies over EASE were actually moderated by the occurrence of only a rather weak IOZM
386 event. Nevertheless, the anomalously wet conditions led to strong groundwater recharge over
387 the EASE domain as evidenced from GRACE. At our study site, the Makutapora wellfield in
388 Tanzania, 2015-16 the strong El Niño-related rainfall reversed a long-term decline in in-situ
389 observed groundwater storage where pumping is intensive and had recently increased. Changes
390 in GWS estimated from an ensemble of GRACE and LSMs also reflect the occurrence of
391 substantial groundwater recharge in 2015-16 and indicate annual groundwater recharge across
392 the region. Broadly, the analysis reinforces the importance of large-scale climate events in
393 driving episodic recharge, critical to replenish heavily exploited aquifers.

394

395 Over SA, the 2015-16 El Niño was associated with extreme drought, the strongest within the
396 observed 116-year record, with an estimated return period of ~260 years, resulting from
397 exceptionally low rainfall and high temperatures. The drought resulted in groundwater storage
398 declines through most of the wet season at our Limpopo study site, with strongly reduced
399 recharge experienced, the second lowest on record. Furthermore, this followed a dry year 2014-
400 15 leading to two consecutive years of low recharge and the greatest recession on record.
401 Clearly, groundwater provides a valuable buffer for periods of reduced surface water
402 availability in drought conditions, although as our results at Limpopo show, consecutive dry
403 years lead to marked storage reduction. Climate projections suggest reduced early season
404 rainfall across much of SA (Lazenby *et al.* 2018) compounding rising temperatures, and the
405 implications of this for climate resilience require a better understanding of these impacts on
406 groundwater recharge as well as surface water resources.

407



GRACE data and LSM outputs are clearly useful in complementing in-situ data, but a number of issues emerge. Although at the broadest scale the GRACE Δ GWS anomalies in 2015-16 are consistent with rainfall anomalies, there are a number of apparent inconsistencies over quite large areas. Resolving the underlying reasons for these is problematic, but likely candidates include the effects of poor climate data over Southern Africa, influencing and compounded by uncertainties in Δ SMS and Δ SWS estimates simulated by land surface models, on which the estimation of GRACE Δ GWS depends. When averaged over comparable scales at Limpopo GRACE and piezometry agree well, at least for seasonal averages. Comparison with the local observations shows that GRACE GWS estimates are considerably noisier, especially at Makutapora where the spatial averaging scale of in-situ data and GRACE differ greatly. Local groundwater abstractions are apparent in the Makutapora record and very likely at Limpopo.

Our results highlight the potential for adaptive strategies, such as managed aquifer recharge, for optimising the capture or storage of episodic recharge in East Africa during El Niño and/or positive IOZM events, and by corollary over Southern Africa during La Niña events (given the opposing dipole structure of ENSO-related rainfall anomalies across SA/EASE). Of course other modes of climate variability driving rainfall extremes are also important. Such interventions can enhance the positive role of groundwater in climate-resilient water and drought management. At Makutapora, managed aquifer recharge exploiting El Niño and/or positive IOZM events may contribute to resilient urban water supply systems for the city of Dodoma. Our findings strengthen the case for a greater understanding of the drivers of rainfall extremes over Africa and their relationship with recharge processes under past, current and future climates and at various temporal and spatial scales. Such knowledge is crucial to inform water management policies and practices for sustainable and climate resilient development in a region undergoing rapid development of groundwater resources.

433

5. Acknowledgements

435

This project was supported by the following research grant awards, funded by the UK Natural Environment Research Council (NERC) and Economic and Social Research Council (ESRC) and the UK Department for International Development (DfID): (i) The Unlocking the Potential of Groundwater for Poverty Alleviation (UpGro) consortium project ‘GroFutures’



440 Grant numbers NE/M008207/1 and NE/M008932/1 see www.grofutures.org) (ii) The Future
441 Climate For Africa (FCFA) consortium project ‘UMFULA’ grant number NE/M020258 (see
442 www.futureclimateafrica.org) (iii) The Science for Humanitarian Emergencies And
443 Resilience (SHEAR) consortium project ‘ForPac’ Grant number NE/P000673/1 and
444 NE/P000568/1 (see www.forpac.org). Further contribution was received from the UK
445 Engineering and Physical Sciences Research Council (EPSRC) ‘Banking the Rain’ grant
446 number 172313 under the Global Challenges Research Fund (GCRF), and The Royal Society
447 Leverhulme Senior Fellowship to RT (Ref. LT170004). MOC is supported by a UK NERC
448 Independent Research Fellowship, grant number NE/P017819/1. *The Chronicles Consortium*
449 (<https://www.un-igrac.org/special-project/chronicles-consortium>), which coordinates long-
450 term groundwater in situ observations was supported by the UK government under the
451 UPGro programme.

452

453



454 6. References

455 Archer, E. R. M., Landman, W. A., Tadross, M. A., Malherbe, J., Weepener, H., Maluleke,
456 P., & Marumbwa, F. M.: Understanding the evolution of the 2014–2016 summer rainfall
457 seasons in southern Africa: Key lessons, *Climate Risk Management*, 16, 22-28, 2017.

458
459 Bindoff, N.L., P.A. Stott, K.M. AchutaRao, M.R. Allen, N. Gillett, D. Gutzler, K. Hansingo,
460 G. Hegerl, Y. Hu, S. Jain, I.I. Mokhov, J. Overland, J. Perlwitz, R. Sebbari and X. Zhang, :
461 Detection and Attribution of Climate Change: from Global to Regional. In: Climate Change
462 2013: The Physical Science Basis. Contribution of Working Group I to the Fifth Assessment
463 Report of the Intergovernmental Panel on Climate Change [Stocker, T.F., D. Qin, G.-K.
464 Plattner, M. Tignor, S.K. Allen, J. Boschung, A. Nauels, Y. Xia, V. Bex and P.M. Midgley
465 (eds.)]. Cambridge University Press, Cambridge, United Kingdom and New York, NY,
466 USA, 2013.

467
468 Berhane, F., & Zaitchik, B: Modulation of daily precipitation over East Africa by the
469 Madden–Julian oscillation, *Journal of Climate*, 27(15), 6016-6034, 2014.

470
471 Blamey, R. C., Kolusu, S. R., Mahlalela, P., Todd, M. C., & Reason, C. J. C: The role of
472 regional circulation features in regulating El Niño climate impacts over southern Africa: A
473 comparison of the 2015/2016 drought with previous events, *International Journal of*
474 *Climatology*, <https://doi.org/10.1002/joc.5668>, 2018.

475
476 Blunden, J., & Arndt, D. S. : State of the Climate in 2016, *Bulletin of the American*
477 *Meteorological Society*, 98(8), Si-S280, 2016.

478
479 Bonsor, H., Shamsudduha, M., Marchant, B., MacDonald, A., & Taylor, R: Seasonal and
480 decadal groundwater changes in African sedimentary aquifers estimated using GRACE
481 products and LSMs, *Remote Sensing*, 10(6), 904, 2018.

482
483 Calow, R. C., MacDonald, A. M., Nicol, A. L., & Robins, N. S. : Ground water security and
484 drought in Africa: linking availability, access, and demand, *Groundwater*, 48(2), 246-256,
485 2010.



486
487 Cuthbert, M. O., Acworth, R. I., Andersen, M. S., Larsen, J. R., McCallum, A. M., Rau, G.
488 C., & Tellam, J. H.: Understanding and quantifying focused, indirect groundwater recharge
489 from ephemeral streams using water table fluctuations, *Water Resources Research*, 52(2),
490 827-840, doi:[10.1002/2015WR017503](https://doi.org/10.1002/2015WR017503), 2016.
491
492 Cuthbert, M. O., Gleeson, T., Reynolds, S. C., Bennett, M. R., Newton, A. C., McCormack,
493 C. J., & Ashley, G. M. : Modelling the role of groundwater hydro-refugia in East African
494 hominin evolution and dispersal, *Nature communications*, 8, 15696, 2017.
495
496 Dunning, C. M., Black, E. C., & Allan, R. P. : The onset and cessation of seasonal rainfall
497 over Africa, *Journal of Geophysical Research: Atmospheres*, 121(19), 2016.
498
499 Ferguson, C. R., Wood, E. F., & Vinukollu, R. K. : A global intercomparison of modeled and
500 observed land-atmosphere coupling, *Journal of Hydrometeorology*, 13(3), 749-784, 2012.
501
502 Holman, I. P., Rivas-Casado, M., Bloomfield, J. P., & Gurdak, J. J. : Identifying non-
503 stationary groundwater level response to North Atlantic ocean-atmosphere teleconnection
504 patterns using wavelet coherence, *Hydrogeology Journal*, 19(6), 1269, 2011.
505
506 Hunter, P. R., MacDonald, A. M., & Carter, R. C. : Water supply and health, *PLoS*
507 *medicine*, 7(11), e1000361, <https://doi.org/10.1371/journal.pmed.1000361>, 2010.
508
509 Jasechko, S., & Taylor, R. G. : Intensive rainfall recharges tropical
510 groundwaters. *Environmental Research Letters*, 10(12), 124015, doi:[10.1088/1748-](https://doi.org/10.1088/1748-9326/10/12/124015)
511 [9326/10/12/124015](https://doi.org/10.1088/1748-9326/10/12/124015), 2015.
512
513 Koster, R. D., Sud, Y. C., Guo, Z., Dirmeyer, P. A., Bonan, G., Oleson, K. W., ... &
514 Kowalczyk, E. : GLACE: the global land-atmosphere coupling experiment. Part I:
515 overview, *Journal of Hydrometeorology*, 7(4), 590-610, 2006.
516



- 517 Kuss, A. J. M., & Gurdak, J. J. : Groundwater level response in US principal aquifers to
518 ENSO, NAO, PDO, and AMO, *Journal of Hydrology*, 519, 1939-1952, 2014.
519
- 520 Lazenby, M. J., Todd, M. C., & Wang, Y. : Climate model simulation of the South Indian
521 Ocean Convergence Zone: mean state and variability, *Climate Research*, 68(1), 59-71, 2016.
522
- 523 MacDonald, A. M., Bonsor, H. C., Dochartaigh, B. É. Ó., & Taylor, R. G. : Quantitative maps
524 of groundwater resources in Africa, *Environmental Research Letters*, 7(2), 024009, 2012.
525
- 526 McMahon, T. A., Finlayson, B. L., Haines, A., & Srikanthan, R.: Runoff variability: a global
527 perspective, In *The Influence of Climate Change and Climatic Variability on the Hydrologic
528 Regime and Water Resources*, Proceedings of the Vancouver Symposium, August 1987.
529 IAHS Publ. no. 168, 1987.
530
- 531 Meyer, R.: Analysis of groundwater level time series and the relation to rainfall and recharge
532 Water Resources Commission (South Africa), report number 1323/1/05, 2005.
533
- 534 Mishra, V., & Cherkauer, K. A.: Retrospective droughts in the crop growing season:
535 Implications to corn and soybean yield in the Midwestern United States, *Agricultural and
536 Forest Meteorology*, 150(7-8), 1030-1045, 2010.
537
- 538 Nicholson, S. E.: Climate and climatic variability of rainfall over eastern Africa, *Reviews of
539 Geophysics*, 55(3), 590-635, 2017.
540
- 541 Owor, M., Taylor, R. G., Tindimugaya, C., & Mwesigwa, D. : Rainfall intensity and
542 groundwater recharge: empirical evidence from the Upper Nile Basin, *Environmental
543 Research Letters*, 4(3), 035009, 2009.
544
- 545 Ropelewski, C. F., & Halpert, M. S.: Global and regional scale precipitation patterns
546 associated with the El Niño/Southern Oscillation, *Monthly weather review*, 115(8), 1606-
547 1626, 1987.
548



- 549 Russo, S., Marchese, A. F., Sillmann, J., & Immé, G.: When will unusual heat waves become
550 normal in a warming Africa?, *Environmental Research Letters*, 11(5), 054016, 2016.
551
- 552 SADC 2016a: SADC regional situation update on El Nino-induced drought, Issue 02, 12th
553 September 2016
554 ,[https://www.sadc.int/files/9514/7403/9132/SADC_Regional_Situation_Update_No-2_16-](https://www.sadc.int/files/9514/7403/9132/SADC_Regional_Situation_Update_No-2_16-09-2016.pdf)
555 09-2016.pdf accessed 30/12/17,2016.
556
- 557 SADC 2016b: SADC Regional Vulnerability Assessment and Analysis Synthesis Report,
558 State of Food Insecurity and Vulnerability in the Southern African Development Community
559 66pp,2016.
560
- 561 Saji, N. H., Goswami, B. N., Vinayachandran, P. N., & Yamagata, T.: A dipole mode in the
562 tropical Indian Ocean, *Nature*, 401(6751), 360, doi:10.1038/43854, 1999.
563
- 564 Scanlon, B. R., Zhang, Z., Save, H., Sun, A. Y., Schmied, H. M., van Beek, L. P., ... &
565 Longuevergne, L. : Global models underestimate large decadal declining and rising water
566 storage trends relative to GRACE satellite data, *Proceedings of the National Academy of*
567 *Sciences*, 201704665, <https://doi.org/10.1073/pnas.1704665115>,2018.
568
- 569 Seneviratne, S. I., Corti, T., Davin, E. L., Hirschi, M., Jaeger, E. B., Lehner, I., ... & Teuling,
570 A. J.: Investigating soil moisture–climate interactions in a changing climate: A review, *Earth-*
571 *Science Reviews*, 99(3-4), 125-161, doi:10.1016/j.earscirev.2010.02.004, 2010.
572
- 573 Shamsudduha, M., Taylor, R. G., Jones, D., Longuevergne, L., Owor, M., & Tindimugaya, C.
574 :Recent changes in terrestrial water storage in the Upper Nile Basin: an evaluation of
575 commonly used gridded GRACE products, *Hydrology and Earth system sciences*, 21(9),
576 4533-4549, <https://doi.org/10.5194/hess-21-4533-2017>,2017.
577
- 578 Siderius, C., Gannon, K. E., Ndiyoi, M., Opere, A., Batisani, N., Olago, D., ... & Conway, D.
579 :Hydrological response and complex impact pathways of the 2015/2016 El Niño in Eastern
580 and Southern Africa, *Earth's Future*, 6(1), doi:10.1002/2017EF000680,2-22, 2018.



581

582 Taylor, R. G., Koussis, A. D., & Tindimugaya, C.: Groundwater and climate in Africa—a
583 review, *Hydrological Sciences Journal*, 54(4), 655-664, 2009.

584

585 Taylor, R. G., Todd, M. C., Kongola, L., Maurice, L., Nahozya, E., Sanga, H., & MacDonald,
586 A. M. : Evidence of the dependence of groundwater resources on extreme rainfall in East
587 Africa, *Nature Climate Change*, 3(4), 374, 2013.

588

589 Van Wyk, E., Van Tonder, G. J., & Vermeulen, D.: Characteristics of local groundwater
590 recharge cycles in South African semi-arid hard rock terrains—rainwater input, *Water*
591 *SA*, 37(2), <http://dx.doi.org/10.4314/wsa.v37i2.65860>, 2011.

592

593 Vicente-Serrano, S. M., Beguería, S., & López-Moreno, J. I. : A multiscalar drought index
594 sensitive to global warming: the standardized precipitation evapotranspiration index, *Journal*
595 *of climate*, 23(7), 1696-1718, 2010.

596

597 Villholth, K. G. : Groundwater irrigation for smallholders in Sub-Saharan Africa—a synthesis
598 of current knowledge to guide sustainable outcomes, *Water international*, 38(4), 369-391,
599 2013.

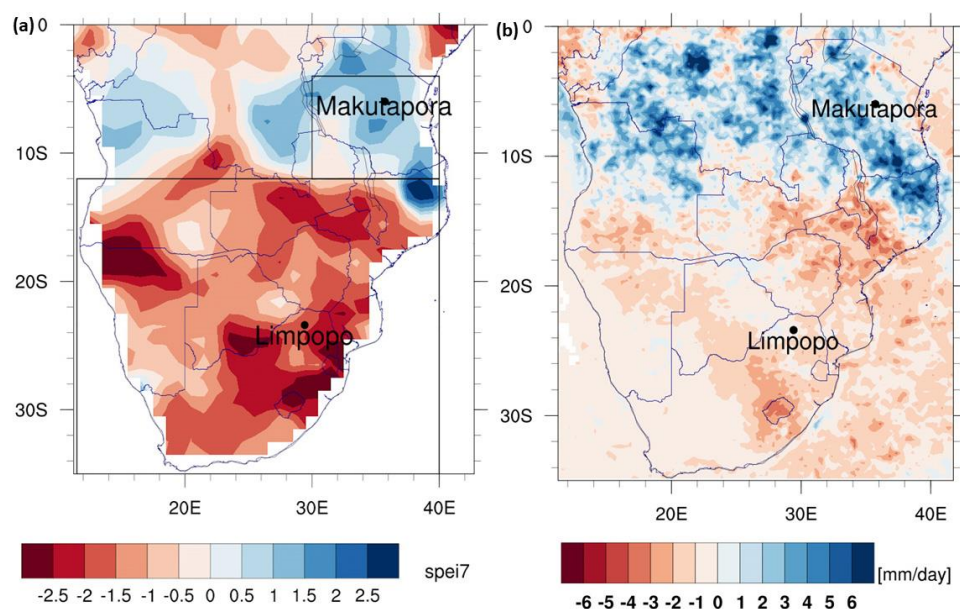
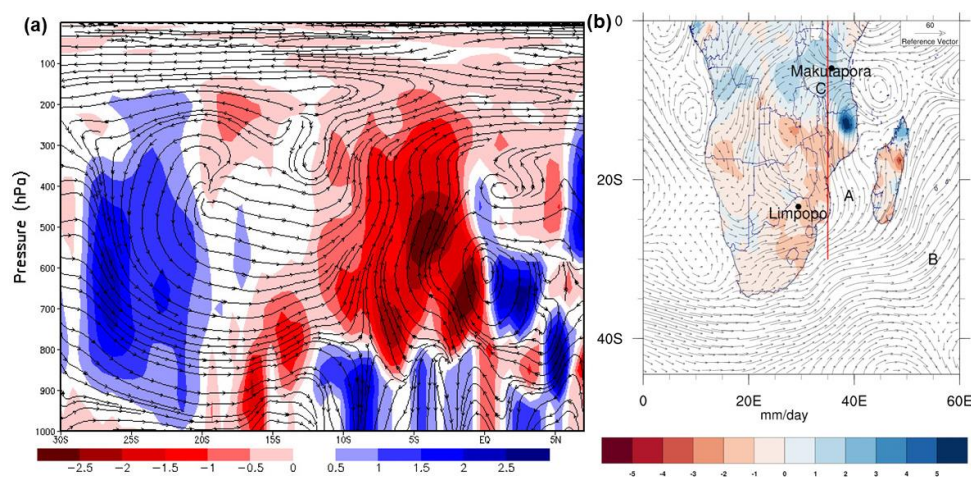


Figure 1. Large-scale climate anomalies over the study region for October-April 2015-16. (a) SPEI-7 (b) Anomalies of the 80th percentile of daily TRMM rainfall (mm day^{-1}). Boxes in (a) show the EASE (small box) and SA (large box) domains used in the SPEI-7 IAF analysis (see Section 2.1 and S3). The piezometer observation locations are also shown.

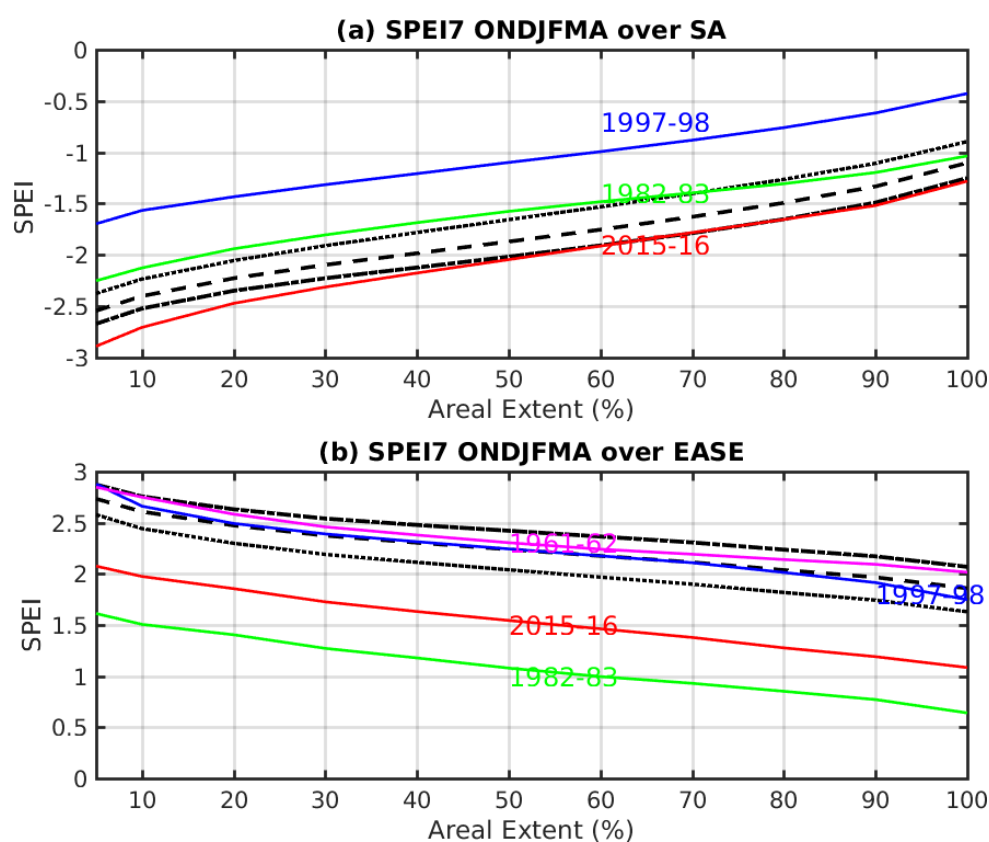


608

609

610

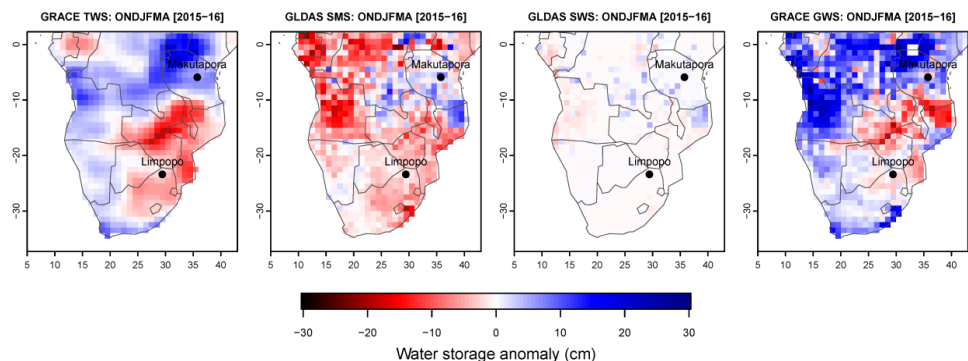
611 Figure 2. Circulation anomalies for October-April 2015-2016. (a) Latitude-height transect plot
 612 of anomalous meridional overturning circulation (streamlines of vertical and meridional wind)
 613 and vertical velocity anomalies (m s^{-1} , shaded) averaged over the 35-37°E. This latitude transect
 614 is shown as a red line on the map in figure 2(b). (b) Vertically integrated moisture flux
 615 anomalies ($\text{g kg}^{-1} \text{m s}^{-2}$, vectors) and rainfall anomalies (mm day^{-1} , shaded).



616

617

618 Figure 3. Intensity-Areal extent-Frequency (IAF) curves (See Section S3 for details of method)
 619 estimated from the seasonal mean SPEI-7 (derived with Penman-Monteith PET, see text for
 620 uncertainty ranges) over (a) the southern Africa domain (10.5°-35.5°S, see box in figure 1a);
 621 (b) the east Africa domain 30°-40°E, 4°-12°S, see box in figure 1a). On the x-axis is the areal
 622 extent over which the SPEI is averaged and the y-axis is the SPEI-7 drought intensity. Solid
 623 coloured lines show the IAF curves for the study El Niño event years; 2015-16 (red), 1997-98
 624 (blue), 1982-83 (green) and (in (b) only) the 1961-62 Indian Ocean Zonal Mode event (purple).
 625 Black lines are the IAF curves for selected benchmark return periods, from top to bottom in (a)
 626 (and bottom to top in (b)), 50 years (dotted), 100 years (dashed) and 200 years (dot-dashed).

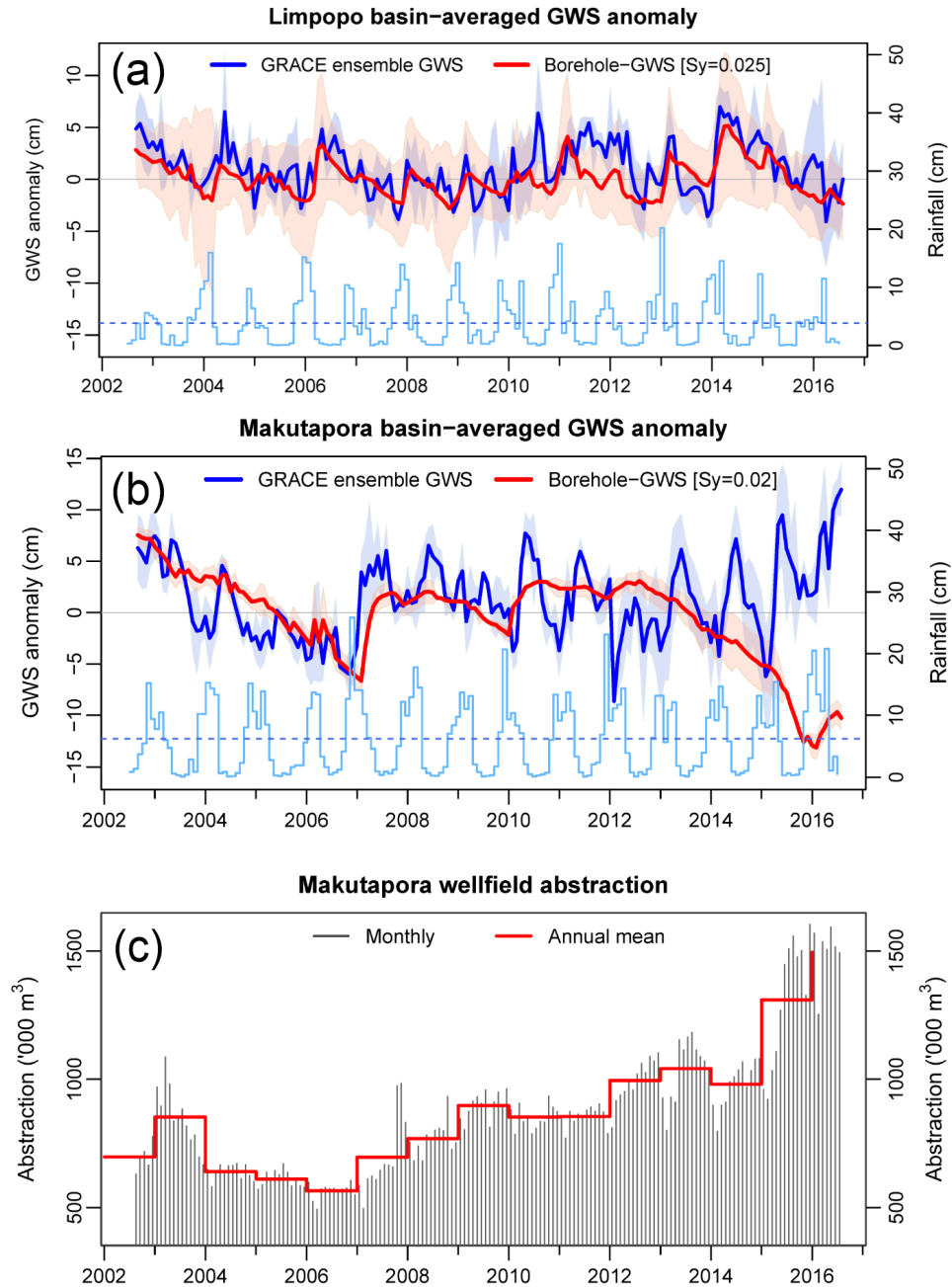


627
628 Figure 4. Water storage anomaly components (cm) over the study domain for the wet season
629 (October-April) of 2015-16 minus long term annual mean 2003-15. (a) GRACE ensemble
630 mean total water storage anomaly (Δ TWS, from CSR, JPL-Mascons, GRGS GRACE
631 products); (b) GLDAS ensemble mean soil moisture storage anomaly (Δ SMS, 4 land surface
632 models: CLM, NOAH, VIC, MOSAIC); (c) GLDAS ensemble mean surface runoff or surface
633 water storage anomaly (Δ SWS, from 4 land surface models: CLM, NOAH, VIC, MOSAIC);
634 and (d) GRACE-GLDAS derived ensemble mean groundwater storage anomaly (Δ GWS, from
635 3 estimates of Δ GWS from 3 GRACE products).

636
637



638



639

640



641 Figure 5. (a) Time series of estimates of monthly Δ GWS anomaly (cm) at Limpopo from
642 August 2002 to July 2016 derived from GRACE averaged over an area approximately ~120
643 000 km² (bold blue line is the mean of CSR, JPL-Mascons and GRGS products, light blue
644 shading representing uncertainty across the three products and four LSMs) and piezometry (red
645 line, mean of all stations, red shading represents uncertainty). Monthly rainfall (from GPCP
646 product, cm) shown as bars with mean monthly rainfall indicated by a dashed line. (b) As (a)
647 but for Makutapora. (c) Monthly groundwater abstraction at Makutapora.